Spectrum of Engineering Sciences
ISSN (e) 3007-3138 (p) 3007-312X
Volume 4, Issue 1, 2026

SYSTEMATIC INVESTIGATION OF THE EFFECT OF γ RADIATION ON THE OPTICAL AND STRUCTURAL PROPERTIES OF NANOSTRUCTURES DOPED WITH IRON-ZINC OXIDE AND GROWN AT LOW TEMPERATURES

[1]Mohammad Asif Syed, [*2]Dr. Barkat Ali Laghari,[3]Qadir Bakhsh Yasir, [4]Sidra Noor Shah, [5]Dr. Mazhar Ali Abbasi, [6]Dr. Yao Hongbing, [7]Zeenat Bibi

[1]*Hohai University, Nanjing China*
[*2]*Department of Physics GC University Hyderabad*
[3]*Hohai University, Nanjing China,*
[4]*Department of Physics, University of Sindh, Jamshoro*
[5]*Department of Physics, University of Sindh, Jamshoro*
[6]*Hohai University, Nanjing China,*
[7]*Department of Physics, University of Sindh, Jamshoro*
[1]asifphy123@gmail.com, [*2]dr.barkatali.laghari@gcuh.edu.pk, [3]qadirbakhsh.yasir@gcuh.edu.pk, [4]sidranoorshah1@gmail.com, [5]mazhar.abbasi@usindh.edu.pk, [6]alenyao@hhu.edu.cn, [7]zenushahid@gmail.com

DOI: https://doi.org/10.5281/zenodo.21890735

Keywords
ZnO nanostructures; ZnO doped with Fe; growth of aquatic chemicals; Gamma radiation; optical zone; Scherer's equation; hexagonal wurtzite; UV-visible spectroscopy; XRD analysis; Effects of radiation

Article History
Received: 03 Jan, 2026
Accepted: 22 Jan, 2026
Published: 25 Jan, 2026

Corresponding Author
Dr. Barkat Ali Laghari

Abstract
In this paper, we present a successful synthesis of Fe-doped nanostructures (ZnO) using the aqueous chemical growth (ACG) method at low temperatures (95°C). Structural, morphological and optical properties were performed on pristine samples of zinc oxide and iron-doped zinc oxide, with iron concentrations of 5%, 10% and 15% respectively. Scanning electron microscopy (SEM) confirmed that all synthesized nanostructures have a hexagonal rod-shaped morphology; however, an increase in the concentration of Fe gradually changes the surface density and leads to agglomeration. The hexagonal crystalline phase of Wurtzit (JCPDS Map No. 36-1451) confirmed X-ray diffraction (XRD) analysis for all samples. The displacement of the diffraction peak (101) to a lower angle shows the successful addition of Fe^{3+} ions to the ZnO lattice, resulting in an increase in the distance d and a reduction in the size of the crystallite. A systematic redshift of the absorption edge and the narrowing of the optical range from 3,392 eV (5% Fe) to 3,225 eV (15% Fe) before irradiation by UV-visible spectroscopy were confirmed. Subsequently, all synthesized samples were subjected to gamma irradiation (γ) at a high dose of 500 gray using a ^{60}Co source at room temperature. Post-irradiation studies showed: (i) In a 15% Fe sample, a blueshift was observed at the absorption edge with area expansion to 3,503 eV; (ii) displacement of the XRD peak at angles higher than 2θ, showing the contraction of the network and the reduction of the distance d; (iii) at certain concentrations, the size of crystallite increases; and (iv) post-irradiation SEM images showed visible surface damage, melting, and destruction of the edges of the nanorods. Fe doping and irradiation γ both lead to a reduction in permeability. This showed that the structural and optical properties of Fe-ZnO can be adjusted by the concentration of dopants and the dose of ionizing radiation. This opens up possibilities for photonic and sensory device applications that harden with radiation.

1. INTRODUCTION

Based on unique, size-dependent physical and chemical properties that differ significantly from their large counterparts, the nanostructures of semiconductor metal oxides have attracted large-scale scientific interest[1], [2]. Zinc oxide (ZnO) occupies a significant position among binary metal oxides due to its direct bandgap (~3.37 eV at 300 K), high exciton energy (60 meV), chemical stability, environmental safety, low production costs, and rich structural diversity [3], [4]. These intrinsic properties make ZnO a highly promising candidate for a wide range of applications, including solar cells, photodetectors, ultraviolet (UV), light-emitting diodes (LEDs), laser diodes, piezoelectric nanogenerators, chemical sensors, photocatalysts, and transparent conductive electrodes [5]–[9].

The exceptional morphological flexibility of ZnO allows its synthesis into various nanostructured forms – nanorods, nanowires, nanotapes, nanoflowers, nanonails, and nanoscales – using various techniques such as pulsed laser deposition (PLD), chemical vapor deposition (CVD), molecular beam epitaxy (MBE), electrodeposition deposition, and solution-based hydrothermal approaches [10]–[13]. In particular, the simplicity of the aqueous chemical growth (GCA) process or the hydrothermal method has made it a very attractive approach, as it has low processing temperature, is scalable, cost-effective, and is compatible with flexible substrates [14]-[15].

Substitution doping of ZnO with TM ions can be used to greatly tailor the electronic and optical properties of the material. Among so many different doping agents studied for ZnO, the one with the closest ionic radius to the ionic radius of the Zn^{2+} ion is the most studied, that is, Fe (Fe^{3+} ratio = 0.645 Å vs. Zn^{2+} = 0.74 Å), which can form effective lattice substitution and introduce localized electronic transitions d-d, which can change optical absorption properties, the luminescence and zonal gap [16]. [17]. The ZnO based systems with Fe-doped are advantageous for multifunctional device applications because of their high photocatalytic activity, superior gas sensation properties and tunability of their optical properties [18].

The interaction of γ beam irradiation with matter can proceed by three main mechanisms: the photoelectric effect, Compton scattering and pair formation [20]. These interactions can result in structure changes, point defects, lattice parameter changes and induce a profound change in the optical/electronic properties of the nanostructured materials. In spite of many studies of Fe doping (ZO), it is relatively rare in the literature to find studies that combine doping with high-dose γ radiation [21].

The present study fills this gap by investigating the combined effects of Fe doping (0%, 5%, 10%, 15%) and high-dose γ irradiation (source 500 Gray, ^{60}Co) on the structural and optical properties of ZnO nanostructures synthesized by the ACG method. Systematic characterization using XRD, SEM and UV-visible spectroscopy is used to establish relationships between structure, properties and radiation, contributing to the fundamental understanding and possible technological applications of these nanomaterials in radiation environments.

2. MATERIALS AND METHODS

2.1 Materials

All of the chemicals used in this study were analytical grade and were purchased from Dae-Jung Chemical Suppliers. The chemicals used were Zinc nitrate hexahydrate [$Zn(NO_3)_2 \cdot 6H_2O$], Hexamethylene etramine (HMT, $C_6H_{12}N_4$), nonhydrated Iron nitrate [$Fe(NO_3)_3 \cdot 9H_2O$] and deionized water (DI). Substrates used to grow on were made of borosilicate glass..

2.2 Substrate Preparation

The glass plates were first cleaned prior to the growth of the nanostructure, to remove contamination on the surface. The cleaning process involved immersing the samples in an isopropanol solution (IPA), then in a sonication bath for 15 minutes, and finally in DI water, which was then dried off at room temperature. This protocol removes any organic or any inorganic contaminant which may prevent uniform growth of the nanostructure.

2.3 Synthesis of Fe-doped ZnO nanostructures using the ACG method

Immaculate, Fe-doped ZnO nanostructures were synthesized using the aqueous chemical growth (ACG) method/the low-temperature hydrothermal method. Equimolar concentrations (0.1 m) of zinc nitrate and HMT were dissolved in 100 mL of DI water with magnetic stirring for 15 minutes until a clear and homogeneous solution was obtained. Doping of Fe was achieved by replacing the corresponding molar fractions of zinc nitrate with iron nitrate to obtain nominal concentrations of Fe of 0%, 5%, 10%, and 15% (molar ratio to zinc). The exact masses of the alloys used are listed in Table 1.

The growing solutions were passed to clean protectors, sealed with aluminum foil to minimize evaporation, and placed in a laboratory convection oven at 95°C for 5 hours. After the end of the growth phase, the samples were allowed to cool to room temperature. The precipitated dusts were collected, filtered through Whatman filter paper and dried. The color of the precipitated powders gradually changed from white (pure ZnO) to light orange and dark orange with an increase in Fe concentration (5%, 10%, 15% Fe), visually confirming the inclusion of iron in the ZnO matrix.

Table 1. *Chemical composition of Fe-doped ZnO synthesis solutions.*

S.No	Fe Conc. (mol%)	$Zn(NO_3)_2$ (g)	HMT(g)	DI Agua (mL)	$Fe(NO_3)_3$ (g)
01	5	1.646	1.050	100	0.0823
02	10	1.646	1.050	100	0.1646
03	15	1.646	1.050	100	0.2469

2.4 Gamma irradiation (γ)

All synthesized, flawless, Fe-doped samples were subjected to gamma irradiation with a ^{60}Co-γ irradiator at the Nuclear Institute of Medicine and Radiotherapy (NIMRA) in Jamshoro, Pakistan. Irradiation was performed at room temperature (27°C) with an absorbed dose of 500 gray (Gy). The dose rate was calibrated using Frickek dosimetry. The temperature of the sample was not significantly affected during irradiation.

2.5 Characterization

Structural characterization was performed by X-ray diffraction (XRD) with an X'Pert PRO analytical diffractometer with CuKα radiation (λ = 1.5421 Å), operating at 40 kV and 30 mA and sampled from 2θ = 20° to 60°. The average size of crystallite was calculated using the Scherer equation:

$$D = (0.9 \times l) / (\beta \times \cos \theta)$$

where D is the average size of the crystal light, λ is the wavelength of the X-rays, β is the total width at half the maximum (FWHM) of the diffraction peak (in radians), and θ is the Bragg angle.

The surface morphology was investigated by scanning electron microscopy (SEM) at different magnifications (×1,000 to ×10,000) by detection of secondary electrons. Energy dispersive X-ray (EDX) analysis confirmed the elemental composition. Optical measurements (absorption and transmissance) were performed with a Jasco V-670 dual-arc UV/VIS spectrophotometer in the wavelength range of 300–800 nm. The optical range (Eg) was calculated from the wavelength at the absorption edge with the current ratio and the ratio Eg = hc/λ, where h is Planck's constant and c is the speed of light.

3. RESULTS AND DISCUSSION

3.1 X-ray Diffraction (XRD) Analysis

3.1.1 Pure ZnO

Fig. 1 presents the XRD model of young ZnO nanostructures grown using the ACG method. The diffraction peaks observed around 2θ = 31.7°, 34.4°, 36.2° and 47.5° correspond to the crystalline planes of the hexagonal structure Vurzite-ZnO (JCPDS map no. 36-1451). The dominant diffraction peak (101) confirms the preferred growth of ZnO nanostructures in the direction of the c-axis perpendicular to the substrate plane. The absence of secondary-phase peaks confirms the high purity of synthesized pure ZnO.

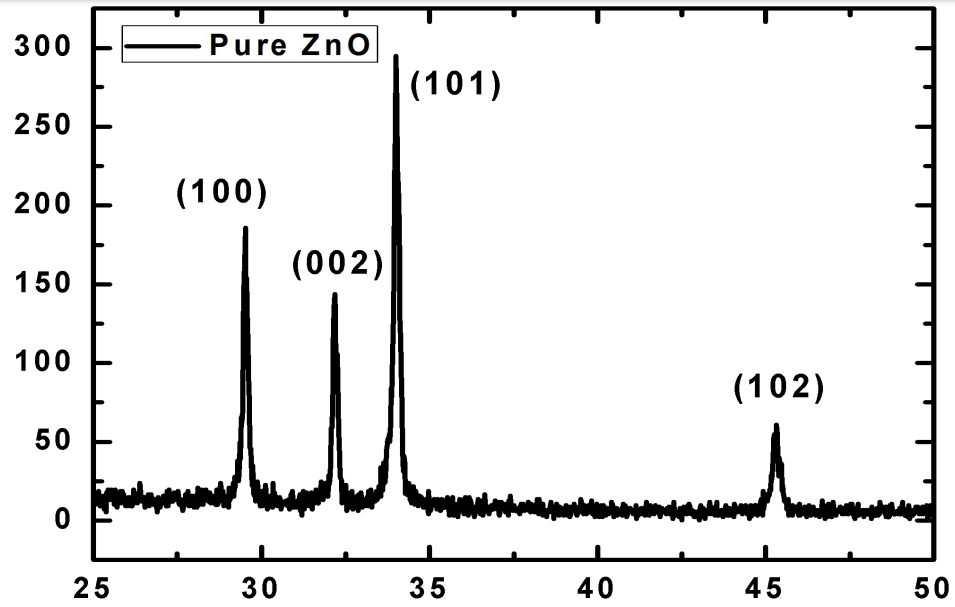

Figure.1. XRD models of young ZnO nanostructures show large (100), (002), (101) and (102) reflections of the hexagonal phase of wurtzite.

3.1.2 Fe-doped ZnO nanostructures (pre-irradiation)

The XRD sample models with Fe-doped ZnO (5%, 10%, 15%) are shown in Fig. 2. All doped samples retain the hexagonal crystal structure of wurcite, confirming that Fe doping does not cause phase transformation. However, several systematic modifications have been observed with the increase in the content of Faith:

- The diffraction peak (101) gradually shifts to lower angles of 2θ as the concentration of Fe increases, indicating an increase in the interplanar distance d. This supports the replacement of smaller Zn^{2+} ions (r = 0.74 Å) with slightly larger Fe^{3+} ions (r = 0.645 Å for octahedral coordination), which can cause local lattice distortions.
- The expansion of the tip increases with Fe, indicating a decrease in crystallite size and/or greater deformation of the lattice.
- The maximal intensity decreases monotonically with an increase in Fe doping, indicating a decrease in crystallinity.

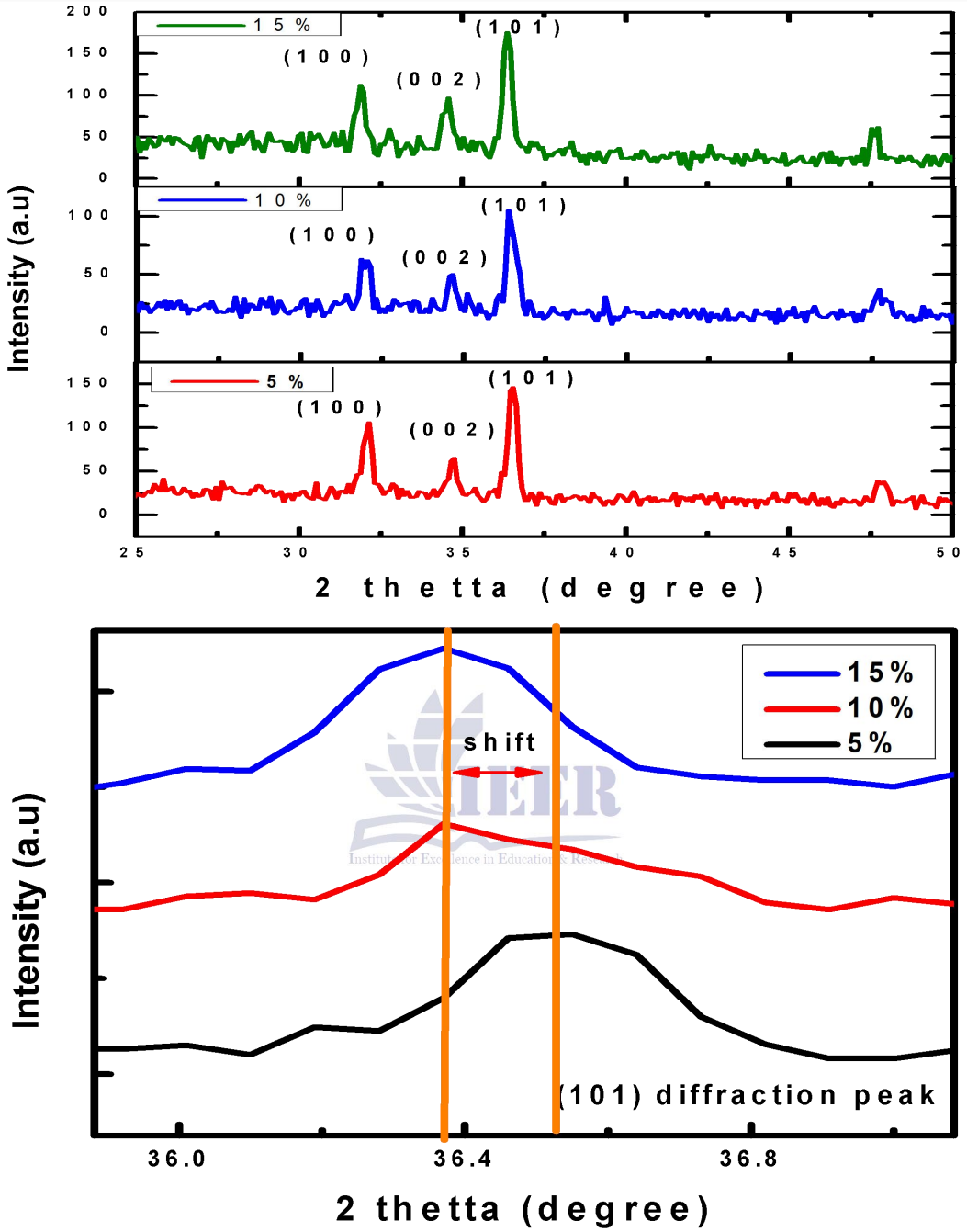

Figure.2. XRD models of Fe-doped ZnO nanostructures, with concentrations of 5%, 10%, and 15% Fe before irradiation, show a systematic shift from peaks to lower angles.

3.1.3 Nanostructures with Fe-doped ZnO (after γ irradiation)

Post-irradiated XRD models (Fig. 3) show significant structural changes induced by 500 Gy γ dose beams. In contrast to the pre-irradiation behavior, the diffraction peaks of the irradiated samples were shifted to higher angles of 2θ compared to their non-irradiated doped counterparts, indicating a contraction of the d-distance.

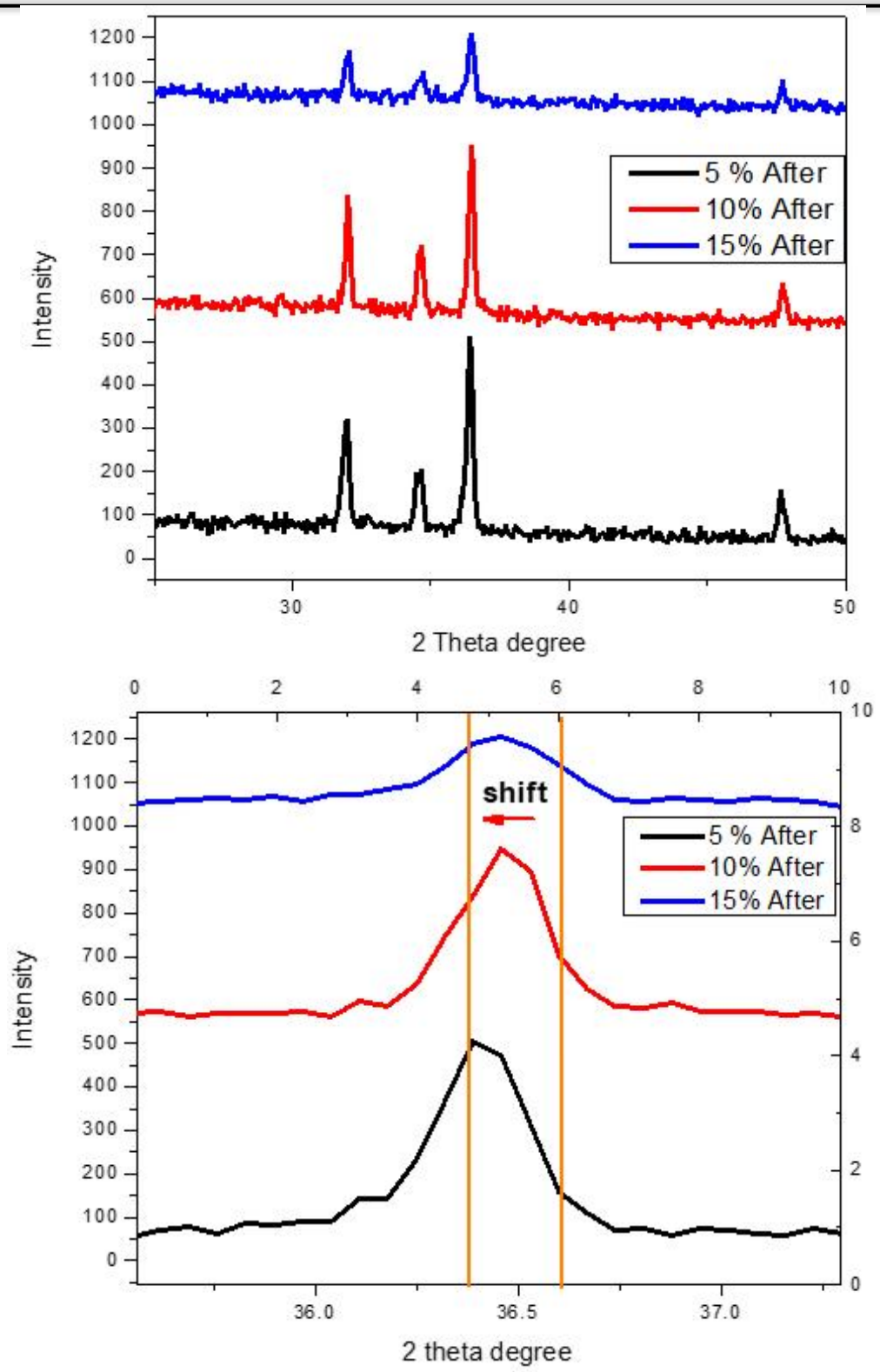

Figure.3. XRD spectra of Fe-touched ZnO nanostructures after γ irradiation (500 Gy) show a maximum shift towards higher 2θ angles compared to preliminary irradiation models.

This can be explained by radiation-induced compaction of the lattice, annihilation of intermediate defects, or partial restoration of radiation damage along the boundaries of the crystalline grains. A comparison of XRD before and after irradiation for the three Fe concentrations is shown in Fig. 4.

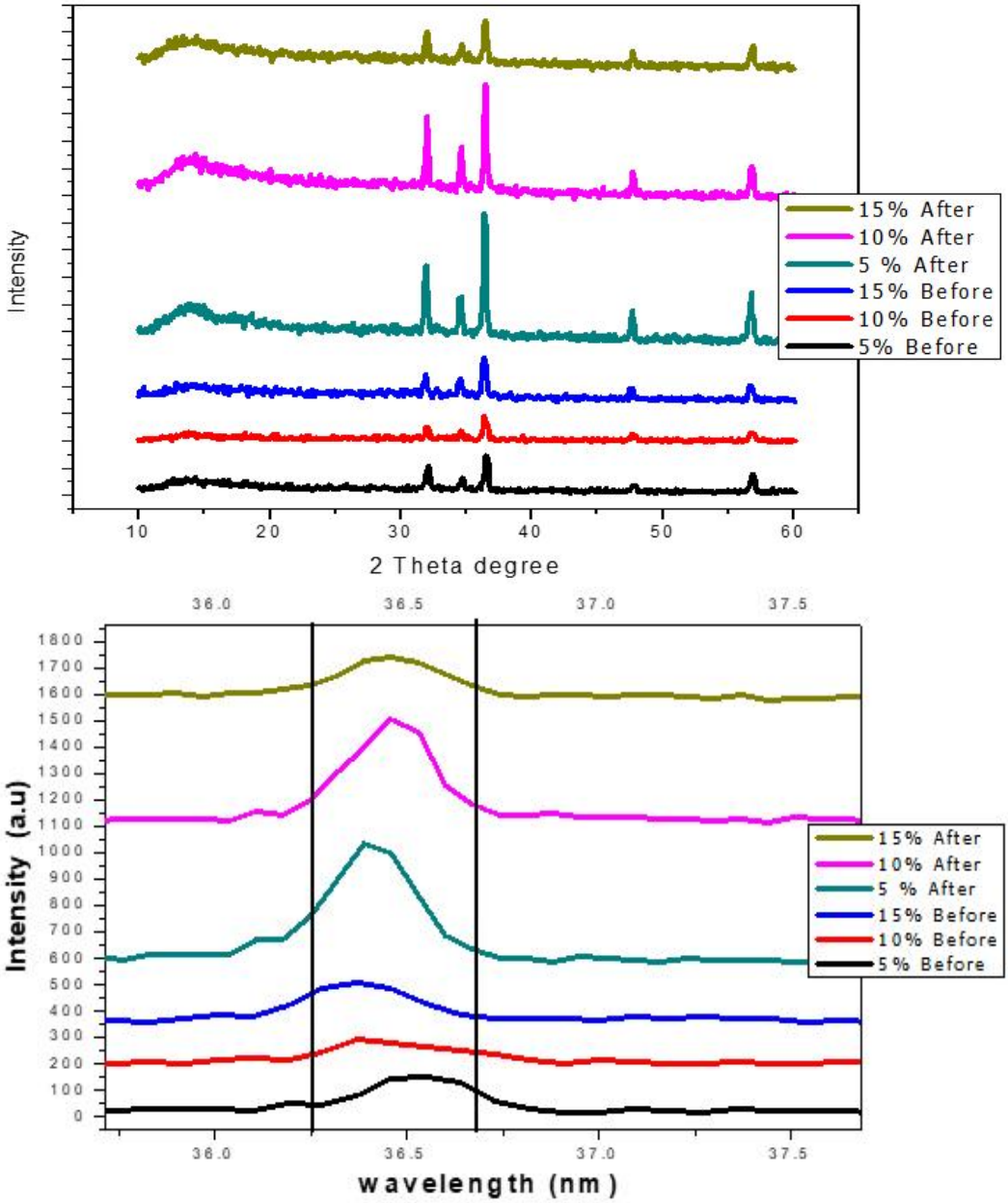

Figure.4. Comparative XRD models of Fe-doped ZnO nanostructures before and after γ irradiation, showing both the full spectrum and the maximum magnification range (101).

3.1.4 Calculation of the magnitude of crystallite (Scherer's equation)

Table 2 summarizes (101) the peak positions, FWHM values, and calculated crystal sizes (D) for all samples before and after irradiation.

Table 2. *Structural parameters of Fe-doped ZnO nanostructures before and after γ irradiation, obtained by XRD analysis using the Scherer equation (λ = 1.5421 Å).*

Extract (Fe%)	Condition	First position (2nd, °)	FWHM β (°)	Crystal Size D (nm)	Δ D (nm)
5%	Predi Irr.	36.531	0.269	77.9	–
5%	The trail of Irr.	36.407	0.230	95.2	+17.3
10%	Predi Irr.	36.459	0.321	66.9	–
10%	The trail of Irr.	36.460	0.216	99.4	+32.5
15%	Predi Irr.	36.373	0.263	84.3	–
15%	The trail of Irr.	36.520	0.320	65.7	−18,6

The data in Table 2 show complex radiation-dependent behavior. In samples doped with 5% and 10% Fe, the size of the crystallite increases after γ irradiation, suggesting radiation-induced growth or fusion of the grains. In contrast, the 15% Fe-doped sample showed a slight decrease in crystal size after irradiation, possibly due to fragmentation by radiation damage at high concentrations of doping-induced defects.

3.2 Surface morphology: SEM analysis

Fig. 5 shows SEM images of pure ZnO at low (×1,000) and high (×5,000 and ×10,000) magnifications prior to irradiation. The images show a dense and uniform arrangement of hexagonal structures in the form of nanorods, confirming the expected morphology of würtzite crystals. Nanorods possess flat, well-defined hexagonal terminal veins that are characteristic of c-oriented ZnO growth.

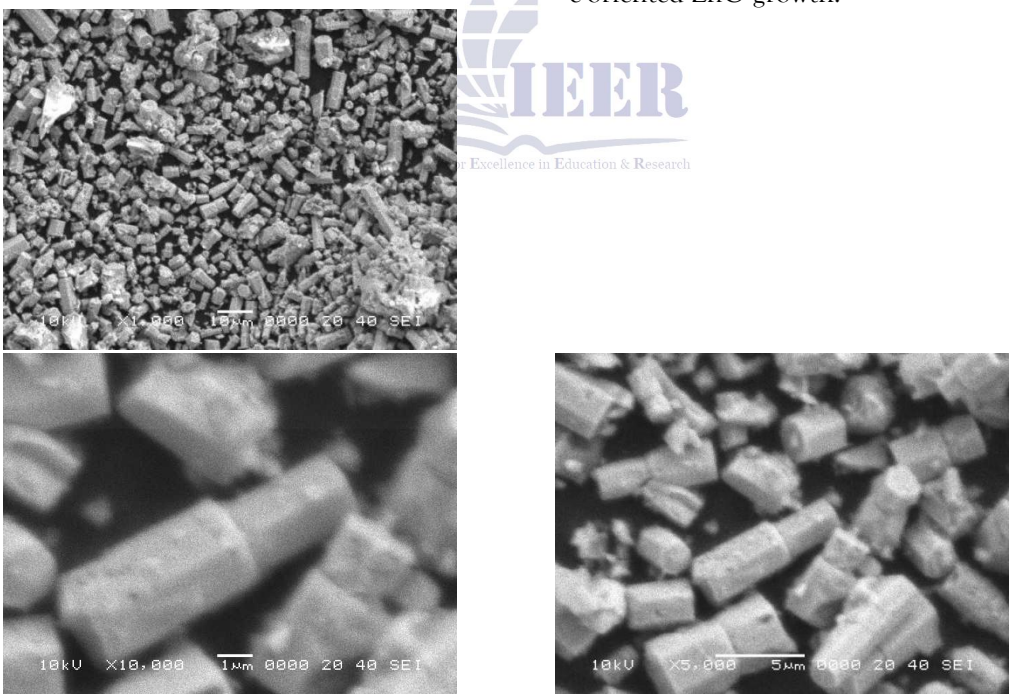

Figure.5.SEM images of flawless ZnO nanostructures prior to irradiation at (a) ×1,000, (b) ×10,000, and (c) ×5,000x magnification, revealing the morphology of the hexagonal rod.

Fig. 6(a)–(c) shows SEM images of ZnO in contact with Fe at concentrations of 5%, 10%, and 15% Fe. The morphology of the hexagonal rod is preserved at all levels of alloys; However, systematic changes in surface density and agglomeration are recognized. At 5% Fe (Fig. 6a), the nanorods show a slight surface roughness compared to pure ZnO. At 10% Fe (Fig. 6b), the density of the nanorods

and the change in aspect ratio become more pronounced. Significant agglomeration of nanostructures is also seen on the surface for the 15% Fe (Fig. 6c), indicating that improved doping leads to changes in the uniform growth rate. The observations are similar to those reported in which Fe^{3+} acts as germination sites and changes the crystal growth process in the ACG process [22, 23].

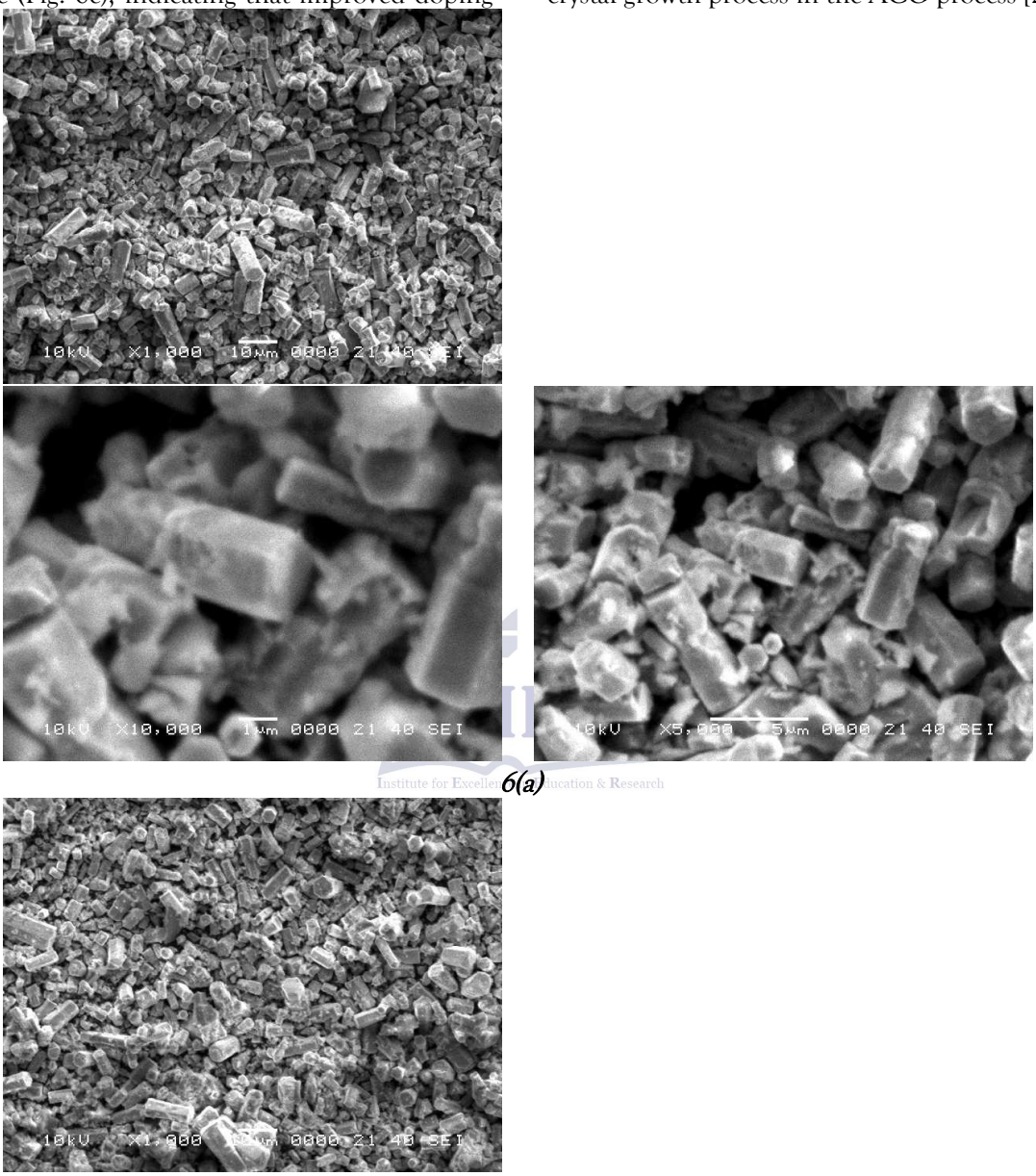

6(a)

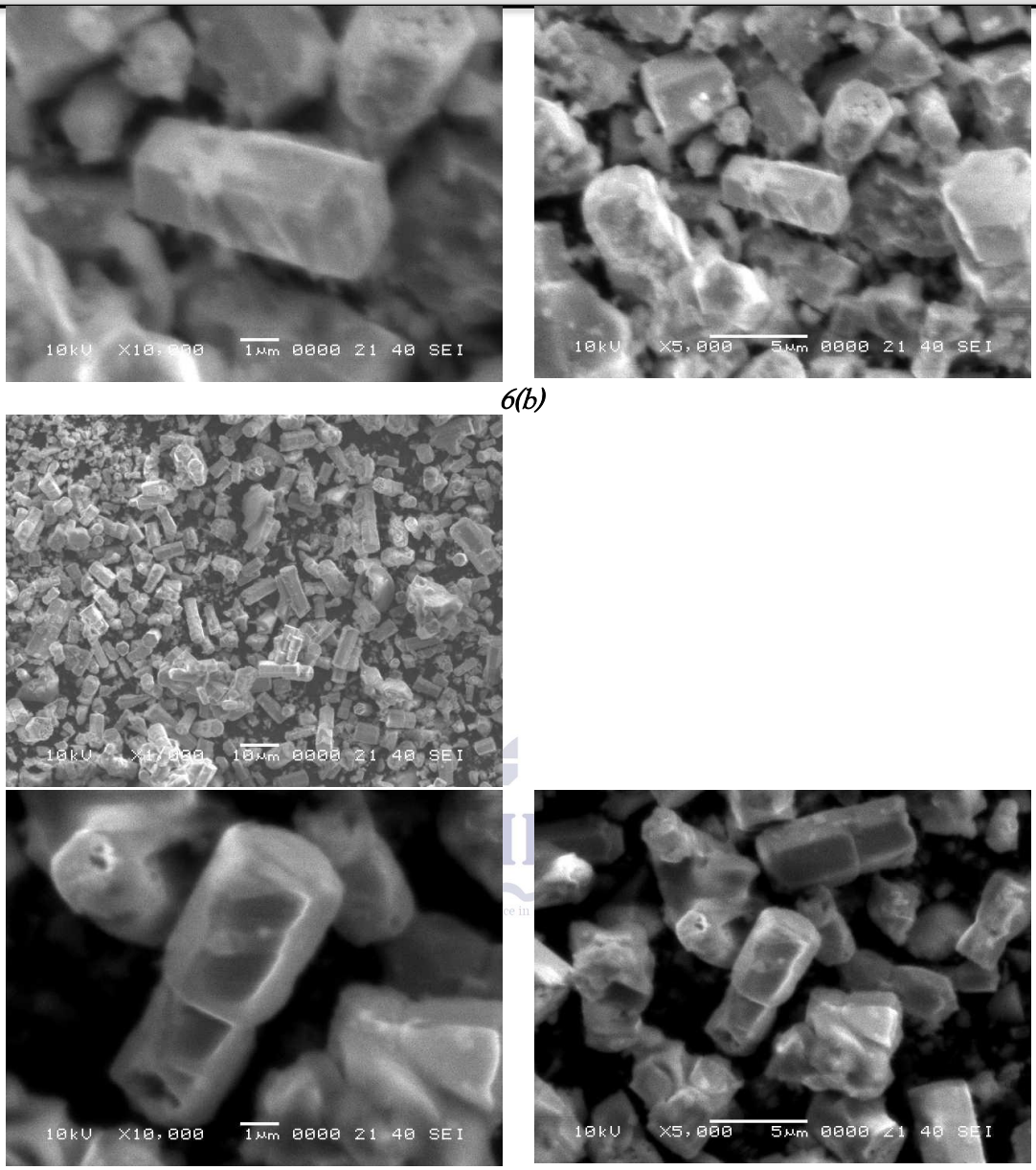

6(b)

6(c)

Figure 6. SEM images of Fe-doped ZnO nanostructures and (a) 5% Fe, (b) 10% Fe, and (c) 15% Fe before γ irradiation. A progressive agglomeration of surfaces is observed.

The SEM images comparing morphologies before and after irradiation (Fig. 7) represent some of the most impressive results of this study. After exposure to 500 Gy γ radiation, the edges of nanobirds appear visibly rounded, eroded and in some regions partially melted. The sharp hexagonal panels observed prior to irradiation are replaced by curved and damaged surfaces. This morphological degradation is attributed to the intense ionizing energy deposited by γ photons through Compton scattering and pair-producing mechanisms that create secondary electron cascades capable of locally fusing nanorod surfaces. These observations have important implications for the radiation hardness of ZnO-based devices intended for use in high-radiation environments.

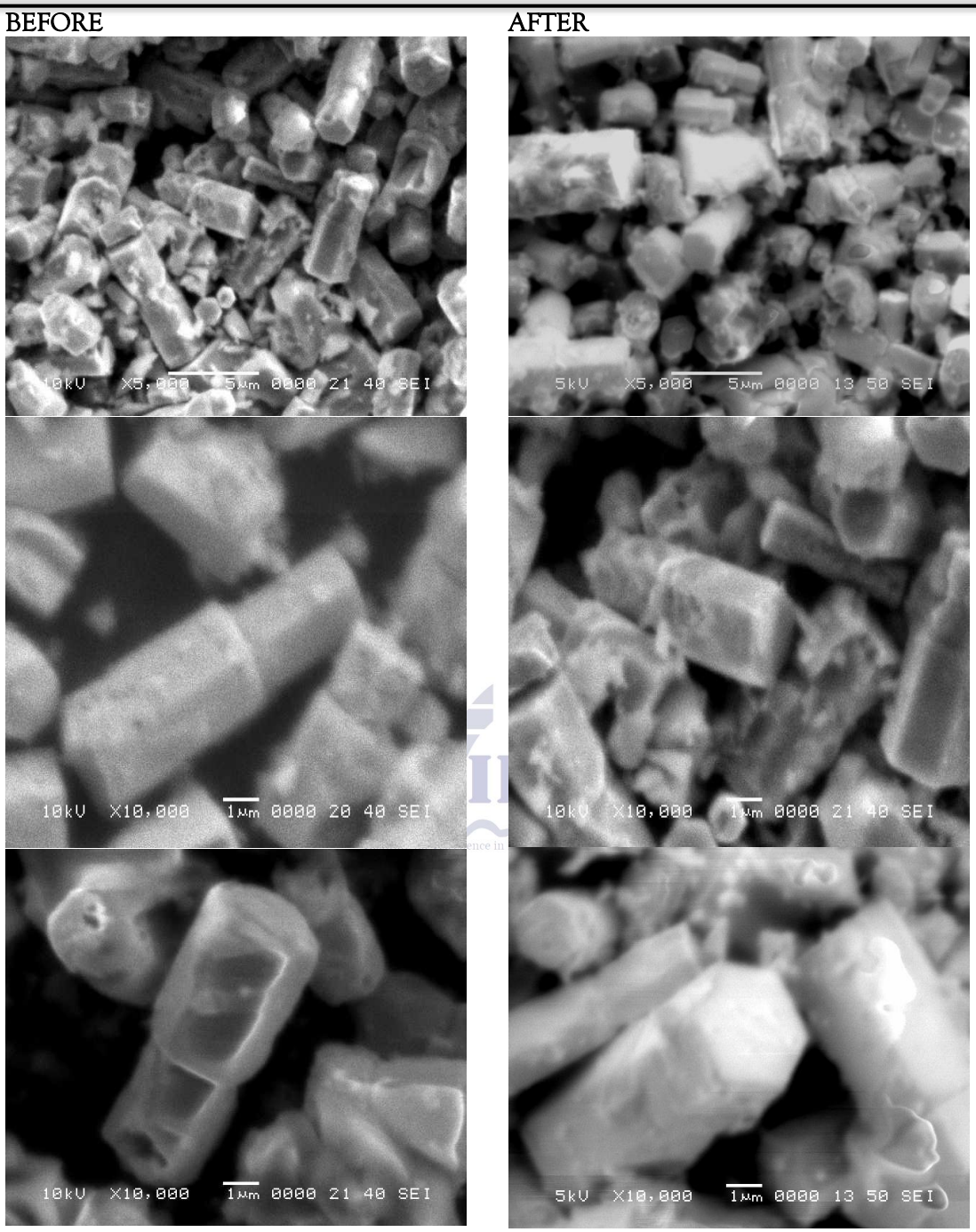

Figure 7.Comparative SEM images of Fe-doped ZnO nanostructures before (left column) and after (right column) γ irradiation at 500 Gy, showing radiation-induced surface damage, edge rounding, and partial nanobar facet fusion.

3.3 Visible UV spectroscopy and optical bandgap

3.3.1 Influence of Fe doping on optical absorption (before irradiation)

Fig. 8 shows the UV-visible absorption spectra of Fe-doped ZnO nanostructures at Fe concentrations of 5%, 10%, and 15% before irradiation. A systematic redshift is observed at the absorption edge with increasing Fe content, which corresponds to a reduction in the optical area. This narrowing of the zone is attributed to sp–d exchange interactions between the ZnO-band electrons and the d electrons of the substituted

Fe^{3+} ions, as well as to the introduction of additional energy states into the region [24]. The calculated values of the area are shown in Table 3.

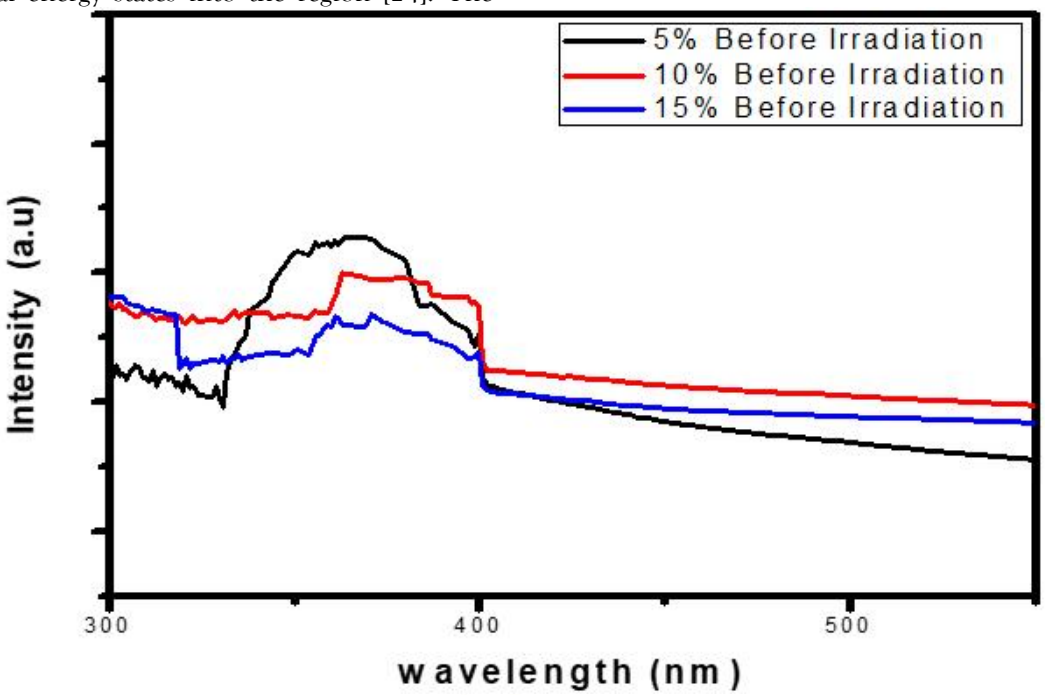

Figure.8. UV-visible absorption spectra of Fe-doped ZnO nanostructures (5%, 10%, 15% Fe) prior to γ irradiation, showing systematic redshift with increasing Fe concentration.

3.3.2 Influence of γ irradiation on optical absorption

Fig. 9 shows the absorption spectra of samples with Fe-doped ZnO after γ irradiation. In stark contrast to the pre-irradiation behavior, the spectra after irradiation show a blueshift at the absorption edge and an increase in optical area values. This blueshift may result from: (i) radiation-induced healing of defects in vacuum oxygens that contributed to conditions in the subbands prior to irradiation; (ii) lattice compaction, which decreases the distance d (confirmed by XRD), which increases the effects of quantum retention; and (iii) partial elimination of Fe doping from replacement sites under intense γ radiation, thereby reducing the interaction between the SP–D exchange [25].

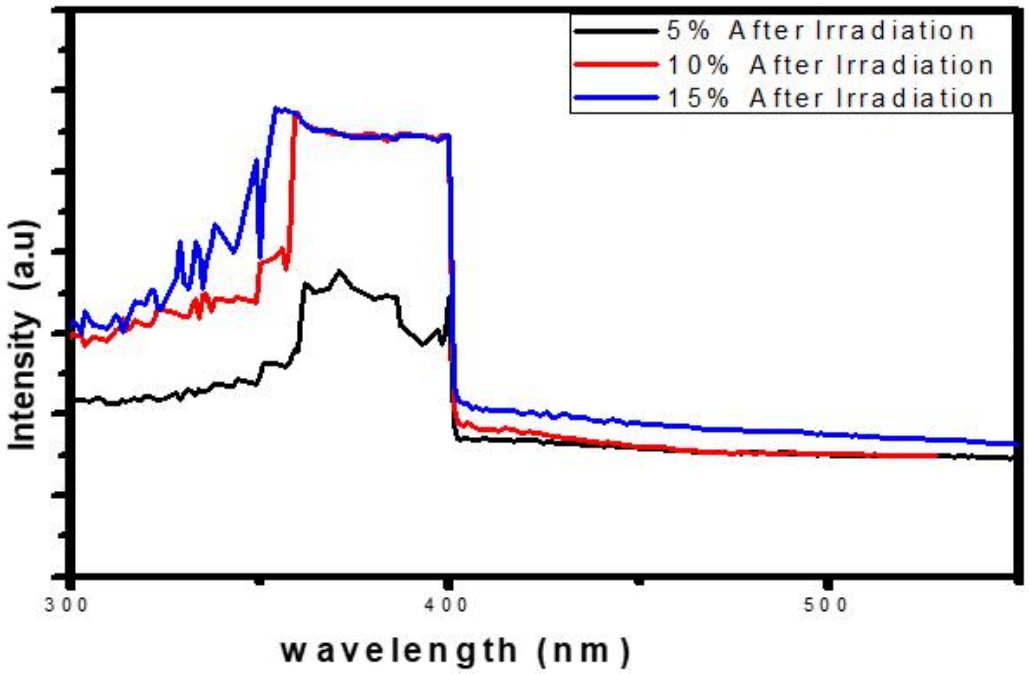

Figure 9. UV-visible absorption spectra of Fe-doped ZnO nanostructures (5%, 10%, 15% Fe) after γ irradiation at 500 Gy, showing a blueshift at the absorption edge.

Table 3. *Optical values of the zone gap of Fe-doped ZnO nanostructures before and after γ irradiation (500 Gy), with differences in zone intermediates.*

S.No	Extract (Fe%)	Max. paragraph λ before Irr. (NM)	Max. paragraph λ trace of Irr. (NM)	Zone Offset (eV)
01	5%	366.6 nm (3.392 eV)	366.2 nm (3.432 eV)	ΔEg = +0.040 eV
02	10%	377.7 nm (3.291 eV)	358.9 nm (3.464 eV)	ΔEg = +0.173 eV
03	15%	385.5 nm (3.225 eV)	354.0 nm (3.503 eV)	ΔEg = +0.278 eV

The data in Table 3 clearly show that the area caused by γ exposure is proportional to Fe's doping concentration: 0.040 eV for 5% Fe, 0.173 eV for 10% Fe, and 0.278 eV for 15% Fe. This concentration-dependent radiation response suggests that highly doped samples are more susceptible to radiation-induced structural changes, providing an adaptable way to shape zoned areas using combined doping and radiation strategies.

3.3.3 Gearbox Analysis

UV-visible transmittance spectra (Figs. 10–12) confirm the absorption results. Fig. 10 compares the permeability of pure ZnO and Fe-doped ZnO before irradiation. Optical transmittance systematically decreases with an increase in Fe content in the apparent wavelength range, which is consistent with an increase in light scattering on the agglomerated surfaces of the nanovarillos and better absorption by Fe^{3+} d–d transitions. After γ irradiation (Fig. 11), permeability decreases further in both intact and Fe-doped samples, suggesting that radiation-induced defects act as additional centers of scattering and absorption. The comparative permeability diagram (Fig. 12) clearly shows that γ irradiated samples have the lowest permeability values, with the Fe irradiated samples showing the greatest reduction.

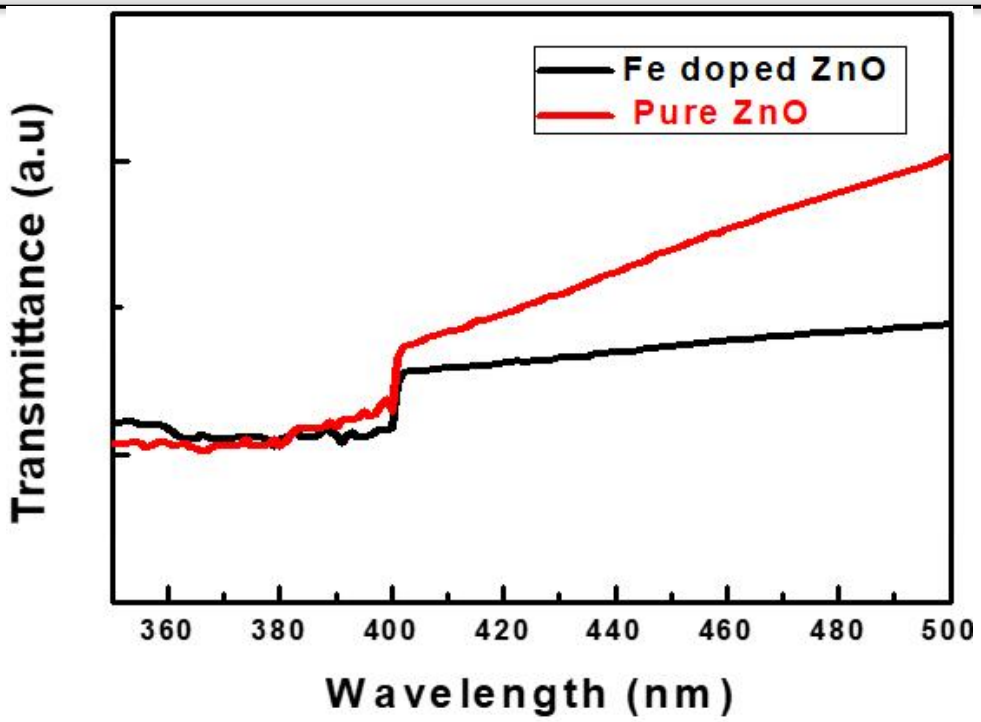

Fig. 10. UV-visible transmission spectra of pure ZnO and Fe-doped ZnO (15% Fe) before γ irradiation.

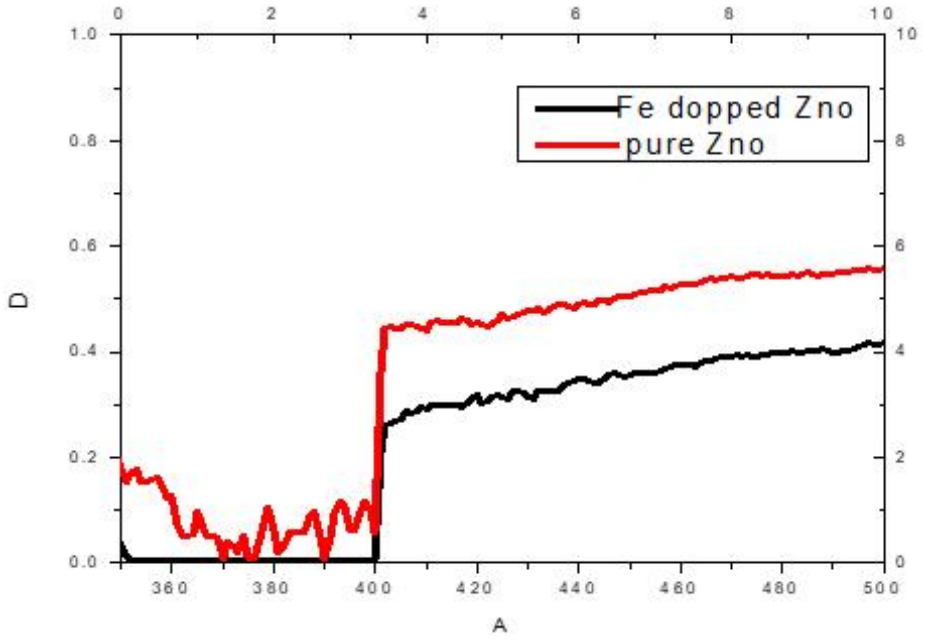

Figure.11. UV-visible permeability spectra of irradiated pure ZnO and Fe-doped ZnO show radiation-induced permeability reduction.

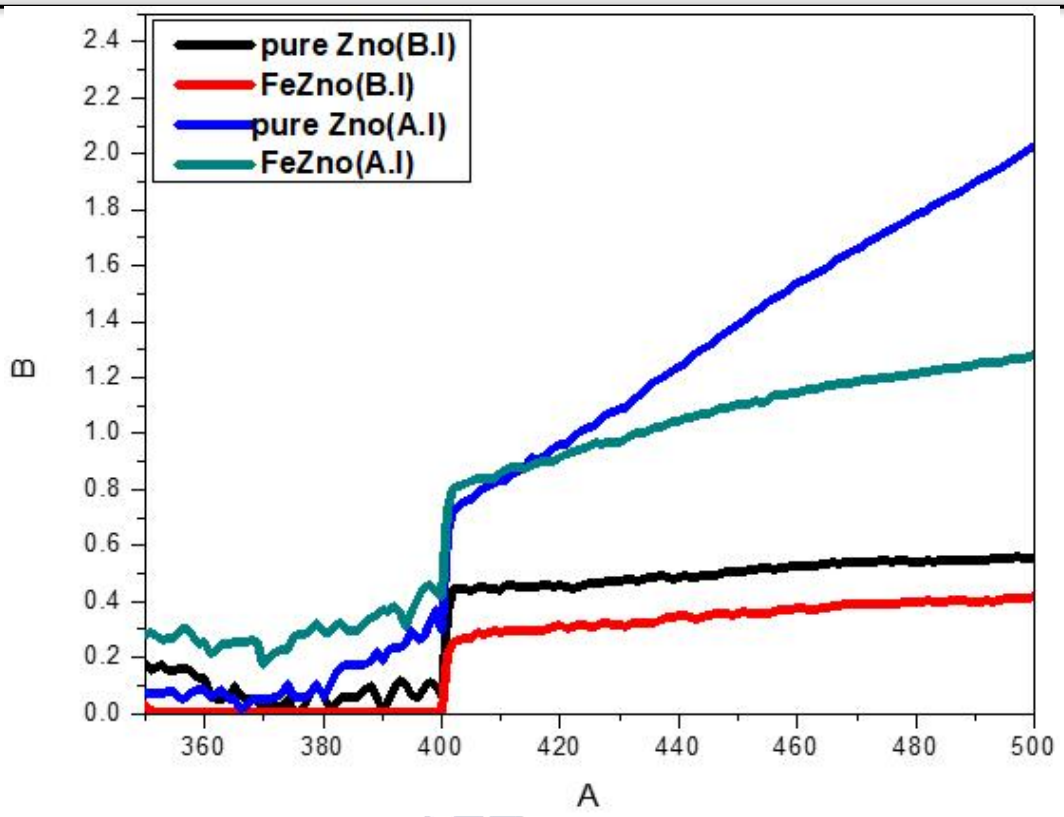

Fig. 12. Normalized UV-visible permeability spectra of pure ZnO and Fe doped ZnO before (B.Irr.) and after (A.Irr.) γ irradiation.

4. CONCLUSIONS

In this work, ZnO nanostructures doped with Fe and their structural and optical properties obtained from the low temperature aqueous chemical growth method are investigated, and the effect of high dose γ irradiation (500 Gy, ^{60}Co) on the structural and optical properties of the Fe-doped ZnO nanostructures is determined. The following are the main findings: The ACG method was found to be effective to obtain hexagonal wurtzite-ZnO nanostructures with rod-like shape at all level of Fe-doping up to 15%. Systematic changes were observed in the positions and intensities of XRD maxima as well as the FWHM values as Fe was introduced, confirming the presence of Fe. Pre-irradiation XRD measurement revealed that the diffraction peak (101) shifted to lower 2θ angle with the increase of Fe content implying the lattice expansion caused by the substitution of Fe^{3+} for Zn^{2+} . Before irradiation, the crystallite sizes (Scherer's equation) vary from about 66.9 nm (10% Fe) to 84.3 nm (15% Fe).

3. UV-visible spectroscopy showed a systematic redshift (narrowing of the zone from 3,392 eV to 3,225 eV) with an increase in Fe content before irradiation, which is due to sp–d exchange interactions and the formation of sub-area gap states.

4. After γ irradiation at 500 Gy, the XRD peaks are shifted to higher angles of 2θ, indicating radiation-induced lattice compaction and reduction of the d-distance. Crystallite sizes show concentration-dependent changes, with samples containing 5% and 10% Fe showing radiation-induced grain growth.

5. UV-visible spectra after irradiation show a blueshift at the optical absorption edge, increasing the values of the zone to 3,432 eV (5% Fe), 3,464 eV (10% Fe) and 3,503 eV (15% Fe). Radiation-induced zone shift is concentration-dependent (ΔEg = 0.040–0.278 eV), indicating a radiation-deactivated zone mechanism.

6. SEM analysis after γ irradiation shows visible surface wear, including edge rounding, surface melting, and destruction of sharp hexagonal

nanorod sheets, indicating partial structural damage at a high dose of 500 Gy.

7. Optical permeability decreases continuously with an increase in Fe doping and an increase in γ radiation dose, which is consistent with improved dispersion and absorption by defective centers.

These results represent quantitative structure-property-radiation relationships for Fe-doped ZnO nanostructures and show that combined doping and radiation strategies can be used for zoning and structural planning. The results are of direct importance for the development of ZnO-based radiation-resistant photonic devices, UV sensors, and optoelectronic components for space or nuclear applications. Future research should focus on systematic dose-dependent studies (10 kGy–50 kGy), alternative transition metal dopants (Ni, Co, Mn), and device-level fabrication and testing.

ACKNOWLEDGEMENTS

Dr. Mazhar Ali Abbasi and Dr. Riaz Hussain Mari of Institute of Physics, University of Sindh, Jamshoro have guided and guided the author. Special thanks is due to Dr. Zafar Hussain Ibupoto who helped with the methodology to research method, Prof. Dr. Mohammad Ishaq Abro and Assistant Professor Umair Aftab (Mehran University) for their help in characterization of materials and Mr. Sajjad Ahmed and Mr. Faisal Ali (NIMRA, Jamshoro) for their cooperation in conducting γ irradiation experiments.

References

[1] J. G. Lu, P. Chang, and Z. Fan, "Quasi-one-dimensional metal oxide materials – Synthesis, properties and applications," Mater. Sci. Eng. R Rep., vol. 52, no. 1–3, pp. 49–91, 2006.

[2] C. Klingshirn, "ZnO: Material, physics and applications," ChemPhysChem, vol. 8, no. 6, pp. 782–803, 2007.

[3] Ü. Özgür et al., "A comprehensive review of ZnO materials and devices," J. Appl. Phys., vol. 98, no. 4, p. 041301, 2005.

[4] D. C. Look, "Recent advances in ZnO materials and devices," Mater. Sci. Eng. B, vol. 80, pp. 383–387, 2001.

[5] D. M. Bagnall et al., "Optically pumped lasing of ZnO at room temperature," Appl. Phys. Lett., vol. 70, no. 17, pp. 2230–2232, 1997.

[6] A. Khan et al., "Piezoelectric nanogenerator based on zinc oxide nanorods grown on textile cotton fabric," Appl. Phys. Lett., vol. 101, p. 193506, 2012.

[7] W. J. Beek, M. M. Wienk, and R. A. Janssen, "Efficient hybrid solar cells from zinc oxide nanoparticles and a conjugated polymer," Adv. Mater., vol. 16, pp. 1009–1013, 2004.

[8] G. T. Rao and D. T. Rao, "Gas sensitivity of ZnO based thick film sensor to NH_3 at room temperature," Sens. Actuators B Chem., vol. 55, pp. 166–169, 1999.

[9] D. S. Ginley and C. Bright, "Transparent conducting oxides," MRS Bull., vol. 25, pp. 15–18, 2000.

[10] J. J. Wu and S. C. Liu, "Low-temperature growth of well-aligned ZnO nanorods by chemical vapor deposition," Adv. Mater., vol. 14, pp. 215–218, 2002.

[11] J.-L. Zhao et al., "Structural, optical and electrical properties of ZnO films grown by pulsed laser deposition," J. Cryst. Growth, vol. 276, pp. 507–512, 2005.

[12] D. C. Look et al., "Characterization of homoepitaxial p-type ZnO grown by molecular beam epitaxy," Appl. Phys. Lett., vol. 81, pp. 1830–1832, 2002.

[13] Z. L. Wang, "Nanostructures of zinc oxide," Mater. Today, vol. 7, pp. 26–33, 2004.

[14] L. Vayssieres, K. Keis, S. E. Lindquist, and A. Hagfeldt, "Purpose-built anisotropic metal oxide material: 3D highly oriented microrod array of ZnO," J. Phys. Chem. B, vol. 105, pp. 3350–3352, 2001.

[15] M. Guo, P. Diao, and S. J. Cai, "Hydrothermal growth of well-aligned ZnO nanorod arrays," J. Solid State Chem., vol. 178, p. 1864, 2005.

[16] M. Mehedi Hassan et al., "Effect of size reduction on structural and optical properties of ZnO matrix due to successive doping of Fe ions," J. Lumin., vol. 145, pp. 160–166, 2014.

[17] L. M. Fang et al., "Synthesis, structure and properties of Fe-doped ZnO by chemical coprecipitation," J. Alloys Compd., vol. 454, pp. 261–267, 2008.

[18] S. Baek, J. Song, and S. Lim, "Improvement of the optical properties of ZnO nanorods by Fe

doping," Physica B, vol. 399, pp. 101–104, 2007.
[19] J. Alarcón et al., "Effect of γ-irradiation on the growth of ZnO nanorod films for photocatalytic applications," Appl. Surf. Sci., vol. 364, pp. 49–55, 2011.
[20] H. Cember and T. E. Johnson, Introduction to Health Physics, 4th ed. New York, NY, USA: McGraw-Hill, 2009.
[21] N. Padmavathy and R. Vijayaraghavan, "Enhanced bioactivity of ZnO nanoparticles – an antimicrobial study," Sci. Technol. Adv. Mater., vol. 9, p. 035004, 2008.
[22] L. E. Greene et al., "Low-temperature wafer-scale production of ZnO nanowire arrays," Angew. Chem. Int. Ed., vol. 42, pp. 3031–3034, 2003.
[23] S.-F. Wang et al., "Effect of ZnO seed layers on the solution chemical growth of ZnO nanorod arrays," Ceram. Int., vol. 35, pp. 1255–1260, 2009.
[24] B. Aleman et al., "Iron doped ZnO nanowires grown by evaporation–condensation and intra-ionic luminescence," J. Appl. Phys., vol. 110, p. 014317, 2011.
[25] E. M. Egorova and A. A. Revina, "Synthesis of metallic nanoparticles in reverse micelles in the presence of quercetin," Colloid J., vol. 64, pp. 301–311, 2002.